

Nickel Substitution in Zinc Ferrite Nanostructures Synthesized by Reactive Sputtering

Ashok Singh Mehta, Ramaswami Mukherjee, Vital Kumar Manoo

Department of Physics, Savitribai Phule Pune University, Pune, INDIA

Abstract

This study examined the impact of substituting nickel for iron(III) in the normal spinel ZnFe_2O_4 crystal structure at electrochemical interfaces, either partially or completely. The resulting $\text{ZnNi}_x\text{Fe}_{2-x}\text{O}_4$ nanostructures had a spherical morphology with an average particle size ranging from 15 to 45 nm. Their energy band gaps varied between 2.05 and 3.02 eV. All synthesized materials retained a normal spinel structure, attributed to the octahedral site preference energy (OSPE) of Zn^{2+} , Fe^{3+} , Co^{2+} and Ni^{2+} ions.

Keywords: Zinc ferrite; Nickel ferrite; Nanostructures; Reactive sputtering

Received: 09 January 2025; **Revised:** 01 March 2025; **Accepted:** 15 March 2025; **Published:** 1 April 2025

1. Introduction

Spintronics, or spin electronics, is a field of technology that exploits the intrinsic spin of electrons, along with their charge, to store and process information [1]. Unlike conventional electronics, which rely solely on charge transport, spintronics leverages spin polarization to enhance device performance, enabling faster processing, lower power consumption, and non-volatile memory storage. Key materials include magnetic semiconductors and ferromagnetic metals, with applications in magnetic random-access memory (MRAM), quantum computing, and advanced sensors [2-4]. Spintronic devices, such as spin valves and tunneling magnetoresistance (TMR) structures, are crucial in hard drives, logic circuits, and next-generation computing technologies [5,6].

Zinc ferrite (ZnFe_2O_4) is a versatile spinel-structured material with significant applications in electronics, catalysis, and energy storage [7]. It has a cubic crystal structure where Zn^{2+} ions occupy tetrahedral sites, while Fe^{3+} ions prefer octahedral coordination [8]. ZnFe_2O_4 exhibits semiconducting properties with a band gap ranging from 1.9 to 2.2 eV, making it useful in photocatalysis [9]. It has good thermal stability, moderate electrical conductivity, and ferrimagnetic behavior at low temperatures. ZnFe_2O_4 can be synthesized using various methods, including sol-gel, co-precipitation, hydrothermal, and solid-state reactions. These techniques influence particle size, morphology, and crystallinity [10-12]. Applications of ZnFe_2O_4 span multiple fields, such as gas sensors, lithium-ion batteries, water purification, and magnetic resonance imaging (MRI) [14-17]. It is also employed as a catalyst in environmental remediation and as an electrode material in supercapacitors. Its unique electrical and magnetic properties make it a promising material for future technological advancements [18,19].

Substituting ferromagnetic metallic ions like cobalt (Co^{2+}) and nickel (Ni^{2+}) in ferrite lattice structures significantly alters their magnetic, electrical, and optical properties [20-24]. This substitution modifies the distribution of cations between tetrahedral and octahedral sites, influencing parameters such as saturation magnetization, coercivity, and electrical resistivity. For instance, cobalt substitution enhances magnetic anisotropy, making it useful in high-density recording media, while nickel improves electrical conductivity for microwave and spintronic applications [25-27]. These modifications are crucial for optimizing ferrites in sensors, magnetic storage, catalysis, and biomedical applications, enabling tailored material properties for specific industrial and technological advancements [28-30].

Reactive magnetron sputtering is a powerful technique for modifying ferrite nanomaterials by enabling controlled substitution of Fe^{3+} ions with ferromagnetic metallic ions like Co^{2+} and Ni^{2+} [31]. This process involves sputtering a target material in an oxygen-rich plasma, allowing precise tuning of composition, stoichiometry, and structural properties (see Fig. 1) [32]. By substituting Fe^{3+} with Co^{2+} or Ni^{2+} , the magnetic and electrical characteristics of ferrites can be tailored for applications in spintronics, sensors, and microwave devices [33]. The technique offers uniform thin films, improved crystallinity, and enhanced performance, making it ideal for fabricating high-quality functional ferrite-based nanomaterials with optimized magnetic and electronic properties [34-37].

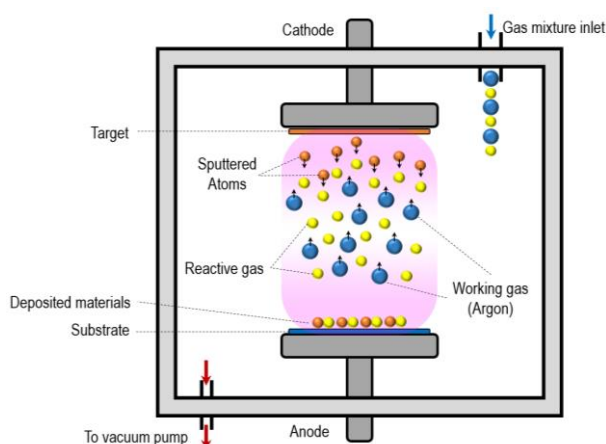


Fig. (1) The principle of reactive sputtering

In this work, the ZnFe_2O_4 nanostructures were synthesized and modified by substitution of Fe^{3+} ions in the ferrite lattice with nickel ions in two consecutive steps using reactive magnetron sputtering technique. The structural and morphological characteristics of the synthesized nanostructures were introduced and studied.

2. Experimental Work

Reactive magnetron sputtering is a widely used thin-film deposition technique for fabricating zinc ferrite (ZnFe_2O_4) and zinc-nickel ferrite ($\text{ZnNi}_x\text{Fe}_{2-x}\text{O}_4$) nanostructures. The process involves the use of a magnetron sputtering system equipped with metallic or composite targets and an oxygen-containing plasma environment to facilitate oxide formation. Figure (2) shows a photograph of the magnetron sputtering system used in this work.



Fig. (2) The DC magnetron sputtering system used in this work

First, the deposition chamber was evacuated to ultra-high vacuum ($\sim 10^{-6}$ Torr) to minimize contamination. Highly-pure Zn, Fe and Ni sheets were used as sputtering targets, and a controlled mixture of argon (Ar) and oxygen (O_2) was introduced to sustain the plasma and produce the oxide compound (ferrite). A DC power supply was applied to the target, generating a plasma that bombards the target material, ejecting atoms that react with oxygen to form ferrite thin films on the substrate. The substrate temperature, sputtering power, gas flow ratio, and deposition time were carefully optimized to achieve the desired stoichiometry and crystalline structure. The deposited films may undergo post-annealing at $500\text{--}800^\circ\text{C}$ in an oxygen atmosphere to enhance phase purity, crystallinity, and magnetic properties. The final nanostructures are characterized using X-ray diffraction (XRD) and field-emission scanning electron microscopy (FE-SEM). This method allows precise control over composition and

morphology, making it an efficient approach for fabricating high-performance ZnFe_2O_4 and $\text{ZnNi}_x\text{Fe}_{2-x}\text{O}_4$ thin films for applications in spintronics, magnetic sensors, and catalysis.

3. Results and Discussion

When nickel is doped into ZnFe_2O_4 to form the $\text{ZnNi}_x\text{Fe}_{2-x}\text{O}_4$ structure, significant changes in the crystalline structure are expected due to the differences in ionic radii and electronic configurations between Ni^{2+} and Fe^{3+} ions. ZnFe_2O_4 typically crystallizes in a normal spinel structure, where Zn^{2+} occupies tetrahedral sites and Fe^{3+} occupies octahedral sites. However, the introduction of Ni^{2+} ions, which have a strong preference for octahedral coordination, can lead to a partial or complete transition to an inverse spinel structure. In this case, Ni^{2+} ions may displace some Fe^{3+} ions from octahedral sites, causing structural rearrangement.

The lattice parameters of the spinel structure are also likely to change due to the smaller ionic radius of Ni^{2+} compared to Fe^{3+} . This substitution can lead to a contraction of the unit cell, resulting in a shift in XRD peaks toward higher angles. However, intermediate compositions ($0 < x < 2$) may exhibit peak shifts toward lower angles, indicating an expansion of the lattice due to the competing effects of Ni^{2+} incorporation and structural distortions. Additionally, the distribution of cations between tetrahedral and octahedral sites can influence magnetic and catalytic properties, as the arrangement of Ni^{2+} and Fe^{3+} ions affects superexchange interactions. These structural modifications make $\text{ZnNi}_x\text{Fe}_{2-x}\text{O}_4$ a versatile material with tunable properties for applications in photocatalysis, magnetism, and photonics.

The XRD analysis was performed to examine the phase compositions and crystallite sizes of the samples. The XRD patterns of $\text{ZnNi}_x\text{Fe}_{2-x}\text{O}_4$ ($x = 0, 0.25, 0.5, 0.75, 1, 2$) are presented in Fig. (3). For $x=0$ and $x=2$, the diffraction patterns align perfectly with those of the normal spinel structures ZnFe_2O_4 and ZnNi_2O_4 . For intermediate compositions, $\text{ZnNi}_x\text{Fe}_{2-x}\text{O}_4$ spinel remains the primary crystalline phase, but the patterns are shifted compared to both ZnFe_2O_4 and ZnNi_2O_4 . Specifically, for x values between 0.25 and 1, the spinel peaks gradually shift toward lower angles as the Ni content increases. This shift suggests that materials with intermediate compositions may adopt a structure that is intermediate between ZnFe_2O_4 and ZnNi_2O_4 nanomaterials.

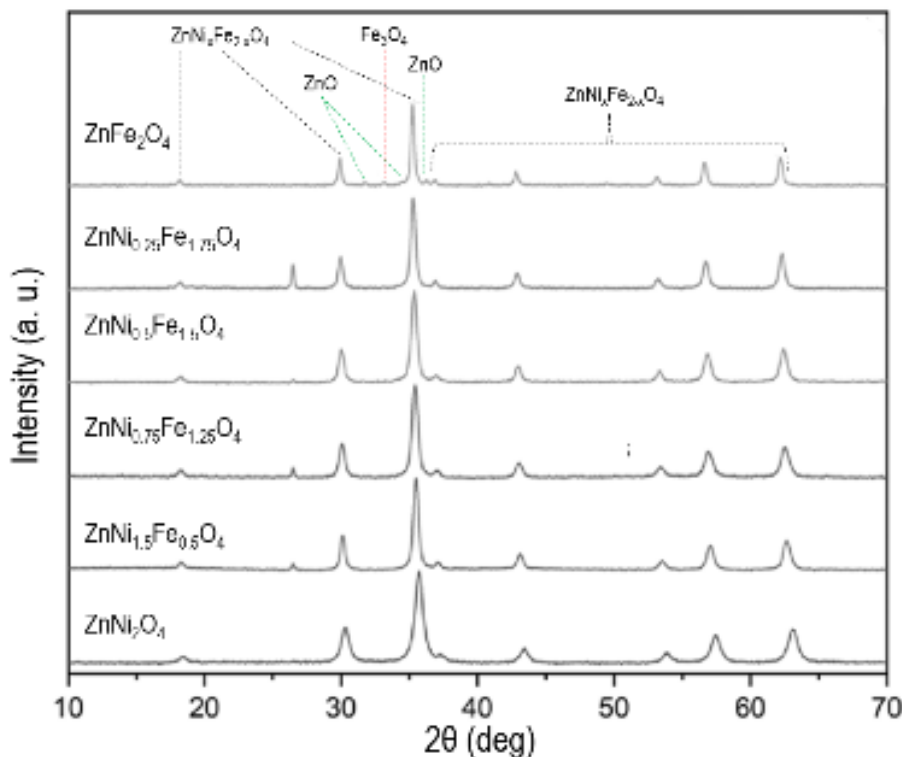


Fig. (3) XRD patterns of the $\text{ZnNi}_x\text{Fe}_{2-x}\text{O}_4$ ($x = 0, 0.25, 0.5, 0.75, 1, 2$) nanostructure samples prepared in this work

The size and morphology of $\text{ZnNi}_x\text{Fe}_{2-x}\text{O}_4$ ($x = 0, 0.25, 0.5, 0.75, 1, 2$) were examined using FE-SEM, as depicted in Fig. (4). The images reveal nanostructured particles with comparable morphologies, along with noticeable particle aggregation. This aggregation arises from the synthesis process, which lacks

precise control over particle size and morphology. The particle size measurements are summarized in table (1). $\text{ZnNi}_x\text{Fe}_{2-x}\text{O}_4$ ($x = 0.25, 0.5, 0.75, 1, 2$) samples exhibited particle sizes similar to those of zinc ferrite ($x = 0$), though the latter showed a slightly larger size. This difference may be attributed to the formation of particles composed of more crystallites in the case of $x = 0$, a result consistent with the synthesis method used.

The surface morphology of $\text{ZnNi}_x\text{Fe}_{2-x}\text{O}_4$ nanostructures plays a critical role in photonics, magnetic, and photocatalytic applications due to its direct influence on material properties. In photonics, a well-defined morphology enhances light absorption and scattering, improving optical performance. For magnetic applications, surface characteristics affect magnetic anisotropy and domain structure, which are vital for data storage and spintronics. In photocatalysis, a high surface area and porous morphology facilitate greater active sites for reactions, enhancing catalytic efficiency and pollutant degradation. Tailoring the surface morphology of $\text{ZnNi}_x\text{Fe}_{2-x}\text{O}_4$ nanostructures thus optimizes their functionality, making them versatile materials for advanced technological applications.

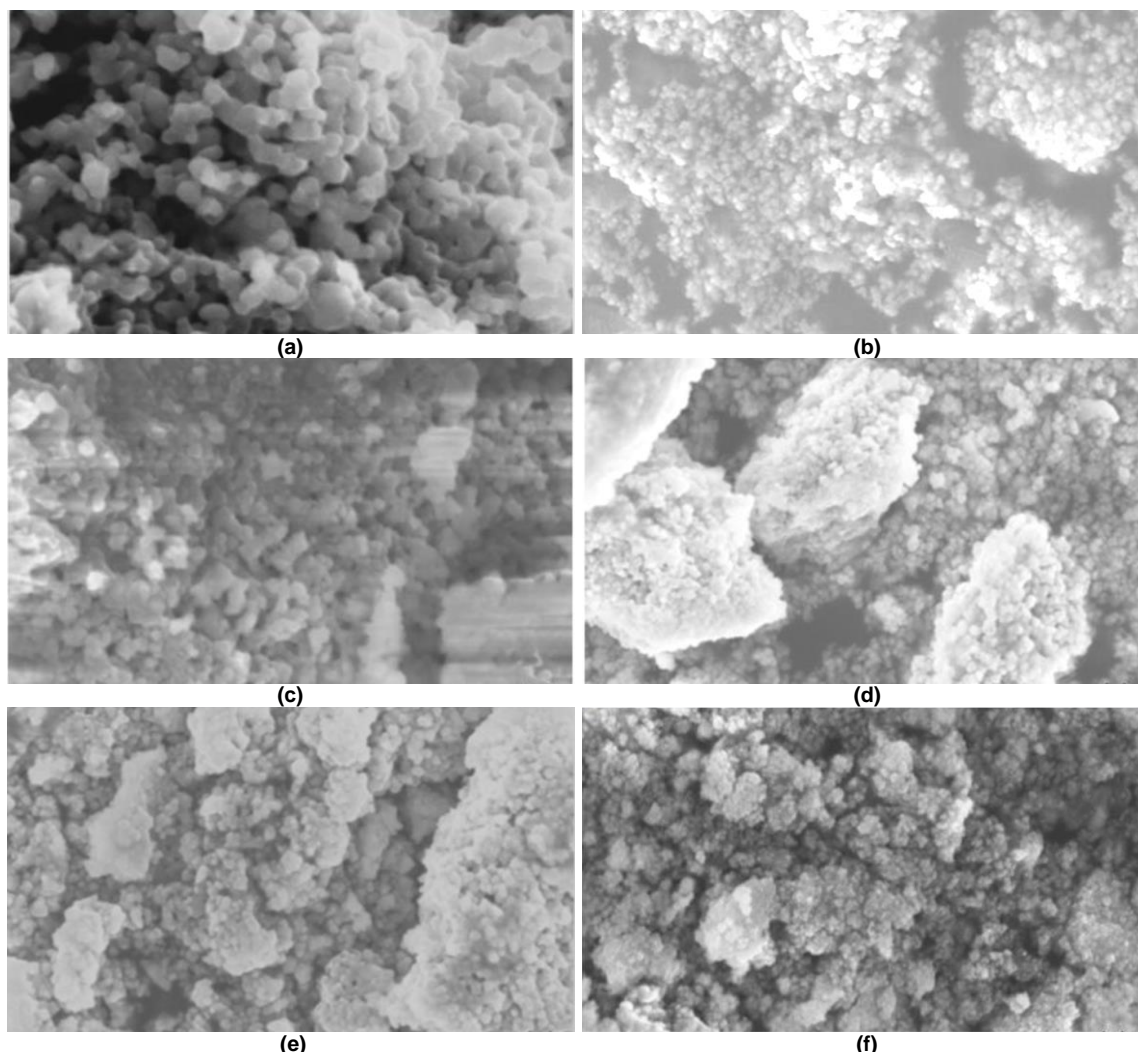


Fig. (4) FE-SEM images of the $\text{ZnNi}_x\text{Fe}_{2-x}\text{O}_4$ ($x = 0, 0.25, 0.5, 0.75, 1, 2$) nanostructure samples prepared in this work

Table (1) The average particle size of the nanostructure samples prepared in this work

Sample	Average particle size (nm)
ZnFe_2O_4	25-60
$\text{ZnNi}_{0.25}\text{Fe}_{1.75}\text{O}_4$	20-35
$\text{ZnNi}_{0.5}\text{Fe}_{1.5}\text{O}_4$	20-25
$\text{ZnNi}_{0.75}\text{Fe}_{1.25}\text{O}_4$	20-30
ZnNiFeO_4	18-30
ZnNi_2O_4	15-25

The concentration of the test sample was varied while cyclic voltammograms were obtained at a constant scan rate of 80 mV/s as shown in Fig. (5). The oxidation current, averaged from three readings at each concentration, was used to create a calibration plot for each sensor. The sensitivity of each sensor, presented in table (2), is represented by the slope of the calibration plot. The ZnFe_2O_4 sensor exhibited the highest sensitivity (38 $\mu\text{A}/\text{mM}$), followed closely by the tailored ZnNiFeO_4 sensor. The limit of detection (LOD) was calculated as $\text{LOD} = \text{KD}/\text{S}$, where K was set to 3 (statistical confidence level), D represents the standard deviation of blank measurements, and S is the sensor's sensitivity. The LOD values for each sensor are shown in table (2). The ZnNiFeO_4 sensor achieved the lowest LOD (1.8 μM), while the ZnFe_2O_4 sensor had the highest LOD (8.0 μM) among the sensors tested.

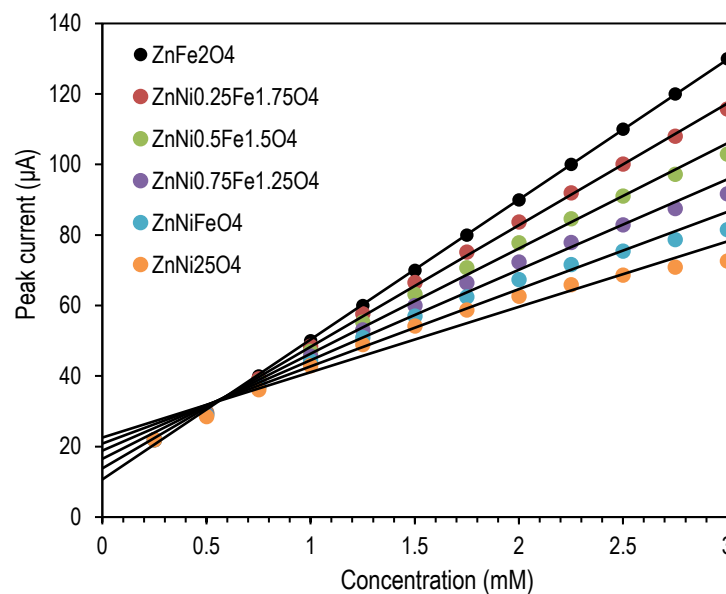


Fig. (5) Calibration of the $\text{ZnNi}_x\text{Fe}_{2-x}\text{O}_4$ ($x = 0, 0.25, 0.5, 0.75, 1, 2$) sensors prepared in this work for the test sample concentration at pH = 77

Table (2) Values of sensitivity and LOD for the $\text{ZnNi}_x\text{Fe}_{2-x}\text{O}_4$ sensors fabricated in this work

Sample	Sensitivity ($\mu\text{A}/\text{mM}$)	LOD (μM)
ZnFe_2O_4	37.5-38.0	7.9-8.0
$\text{ZnNi}_{0.25}\text{Fe}_{1.75}\text{O}_4$	32.0-32.5	7.5-7.7
$\text{ZnNi}_{0.5}\text{Fe}_{1.5}\text{O}_4$	32.5-34.0	2.1-2.3
$\text{ZnNi}_{0.75}\text{Fe}_{1.25}\text{O}_4$	34.0-35.0	2.3-2.4
ZnNiFeO_4	35.5-36.0	1.8-1.9
ZnNi_2O_4	32.0-32.5	2.9-3.0

4. Conclusion

In concluding remarks, the sensitivity of nickel-doped zinc ferrite nanostructures were measured and optimized as a function of the doping level of nickel in the lattice structure of the zinc ferrite. The lattice parameters of the spinel structure are also likely to change due to the smaller ionic radius of Ni^{2+} compared to Fe^{3+} . This substitution can lead to a contraction of the unit cell. The ZnNiFeO_4 sensor achieved the lowest limit of detection (1.8 μM), while the ZnFe_2O_4 sensor had the highest limit of detection (8.0 μM) among the sensors tested.

Reference

- [1] N. Ponpandian, P. balaya, and A. Narayanasamy, J. Phys. Cond. Matter, 14 (2002) 3221.
- [2] A.A. Ahmed, N.A. Dahham, and G.G. Ali, Iraqi J. Appl. Phys., 20(3A) (2024) 505-510.
- [3] M. Madagalam, M. Bartoli, M. Rosito, N. Bkangetti, M. Etzi Collier Pascuzzi, E. Padovano, B. Bonelli, S. Carrar, and A. Tagliaferro, Small Struct., 4(12) (2023) 2300163.
- [4] A.G. Cullis, L.T. Canham, P.D.J. Calcott, J. Appl. Phys., 82 (1997) 909-965.
- [5] A.C.F.M. Costa, E. Tortella, M.R. Morelli, M. Kaufman, and R.H.G.A. Kiminami, J. Mater. Sci., 37(17) (2002) 3569-3572.
- [6] A.K. Al-Kadumi and M. Al-Baghdadi, Iraqi J. Appl. Phys., 20(3B) (2024) 668-670.
- [7] R. Liu, M. Lv, Q. Wang, H. Li, P. Guo, and X.S. Zhao, J. Magnet. Mater., 424 (2017) 155-160.
- [8] B.G. Rasheed, Iraqi J. Appl. Phys., 1(1) (2005) 15-19.

- [9] H. Yamaguchi and S. Murakami, *Nucl. Fusion*, 58(1) (2018) 016029.
- [10] I.N. Yousif, A.T. Abdulhameed, A.M. Essmat, and A.I. Ahmed, *Iraqi J. Appl. Phys.*, 20(3A) (2024) 565-568.
- [11] J. Wang, Y. Xu, W. Li, Y. Yang, and F. Wang, *J. Electrostat.*, 67(5) (2009) 815-826.
- [12] J.N. Jasbijn, T.J. Tibsibim, and G.U. Jasbijn, *Iraqi J. Appl. Phys.*, 18(1) (2022) 27-30.
- [13] M. Jedrusik, M. Głomba, A. Świerczok, J. Mazurek, and P. Halfar, *Int. J. Plasma Environ. Sci. Technol.*, 8(1) (2014) 22-26.
- [14] M.A. Herrero, J. Guerra, V.S. Myers, M.V. Gomez, R.M. Crooks, and M. Prato, *ACS Nano*, 4 (2010) 905-912.
- [15] N. Guettler, P. Knee, Q. Ye, and O. Tiedje, *J. Coat. Technol. Res.*, 17(5) (2020) 1091-1104.
- [16] S.S. Khudiar, U.M. Nayef, and F.A. Mutlak, *J. Nanosci. Nanotechnol.*, 2 (2022) 64-69.
- [17] U.A. Merhan and T.B. Simanja, *Iraqi J. Appl. Phys.*, 18(1) (2022) 31-34.
- [18] X. Zhu, T. Liu, H. Zhao, L. Shi, X. Li, and M. Lan, *Biosens. Bioelectron.*, 79 (2016) 449-456.
- [19] Z. Qu, C. Mao, X. Zhu, J. Zhang, H. Jiang, and R. Chen, *Ind. Eng. Chem. Res.*, 61(36) (2022) 13416-13430.
- [20] A.A. Abbas, S.J. Hasan, I.M. Abdulmajeed, and S.Q. Hazaa, *Iraqi J. Appl. Phys.*, 20(1) (2024) 91-95.
- [21] A.A. Bednyakov, R.A. Gilyarov, O.B. Dzagurov, V.V. Krivolap, and V.S. Kulikauskas, *Instrum. Exper. Tech.*, 41(2) (1998) 284-291.
- [22] A.J. Haider, *Iraqi J. Appl. Phys.*, 4(1) (2008) 37-40.
- [23] A.M. Alwan and O.A. Abdulrazaq, *Int. J. Mod. Phys.* 22 (2008) 417-422.
- [24] A.Yu. Panarin, S.N. Terekhov, K.I. Kholostov, V.P. Bondarenko, *Appl. Surf. Sci.* 256 (2010) 6969-6976.
- [25] F.B. Mohammed Ameen, G.G. Ali, and M.H. Younus, *Iraqi J. Appl. Phys.*, 20(2B) (2024) 321-332.
- [26] H. Yanada, S. Takag, and S. Mamiya, *J. Electrostat.*, 74 (2015) 1-7.
- [27] I.N. Yousif, M.J. Ali, and I.T. Tlayea, *Iraqi J. Appl. Phys.*, 20(3A) (2024) 557-560.
- [28] J. Zhang, Y. Liu, C. Mao, Z. Tang, H. Jiang, W. Xing, and R. Chen, *Chem. Eng. Sci.*, 298 (2024) 120406.
- [29] M. Feidt and D. Paulmier, *Vacuum*, 22(5) (1972) 181-182.
- [30] M. Yamada, S. Seiler, H.W. Hendel, and H. Ikezi, *Phys. Fluids*, 20(3) (1977) 450-458.
- [31] M.V. Chursanova, L.P. Germash, V.O. Yukhymchuk, V.M. Dzhagan, I.A. Khodasevich, and D. Cojoc, *Appl. Surf. Sci.* 256 (2010) 3369-3373.
- [32] T. Zhang, S.A. Liao, L.X. Dai, J.W. Yu, W. Zhu, and Y.W. Zhang, *Sci. China Mater.*, 61 (2018) 926-938.
- [33] R. Molaie, K. Farhadi, M. Forough, and S. Hajizadeh, *J. Nanostruct.*, 8(1) (2018) 47-54.
- [34] S.O. Kasap, A. Bhattacharyya and Z. Liang, *Japanese J. Appl. Phys.*, 31(1R) (1992) 72-80.
- [35] T. Adachi and T. Kawakubo, *Phys. Rev. Special Topics Acceler. Beams*, 16(5) (2013) 053501.
- [36] X. Cui, L. Zheng, Q. Li, and Y. Guo, *Ind. Eng. Chem. Res.*, 62(37) (2023) 14973-14985.
- [37] Z. Cai and S. Park, *Sens. Actuat. B: Chem.*, 367 (2022) 132090.